VIP Lithium-Ion Batteries Very Important Paper

DOI: 10.1002/ange.201404615

Synthesis of Two-Dimensional Transition-Metal Phosphates with Highly Ordered Mesoporous Structures for Lithium-Ion Battery Applications**

Dan Yang, Ziyang Lu, Xianhong Rui, Xiao Huang, Hai Li, Jixin Zhu, Wenyu Zhang, Yeng Ming Lam, Huey Hoon Hng, Hua Zhang, and Qingyu Yan**

Abstract: *Materials with ordered mesoporous structures have shown great potential in a wide range of applications. In particular, the combination of mesoporosity, low dimensionality, and well-defined morphology in nanostructures may exhibit even more attractive features. However, the synthesis of such structures is still challenging in polar solvents. Herein, we report the preparation of ultrathin two-dimensional (2D) nanoflakes of transition-metal phosphates, including $FePO_4$, $Mn_3(PO_4)_2$, and $Co_3(PO_4)_2$, with highly ordered mesoporous structures in a nonpolar solvent. The as-obtained nanoflakes with thicknesses of about 3.7 nm are constructed from a single layer of parallel-packed pore channels. These uniquely ordered mesoporous 2D nanostructures may originate from the 2D assembly of cylindrical micelles formed by the amphiphilic precursors in the nonpolar solvent. The 2D mesoporous $FePO_4$ nanoflakes were used as the cathode for a lithium-ion battery, which exhibits excellent stability and high rate capabilities.*

Control over the morphology, composition, and pore structures of mesoporous materials has proved to be crucial for their applications in catalysis, biosensors, energy conversion, and storage devices, etc.[1] The synthetic methods for preparing the ordered mesoporous materials can be categorized into two general types, known as the hard-template and soft-template methods. The former, which commonly uses siliceous materials as the template, involves the tedious removal of the template with HF or NaOH solution, and thus is not applicable to materials that are sensitive to acid or alkali.[2] The use of different structure-directing agents in latter method allows the generation of ordered mesoporous structures through charge density mapping, hydrogen bonding, or dative coordinate bonding interactions.[3] The polar solvent, such as water, ethanol, formamide, or methanol, normally used in the soft-template methods plays an important role in the formation of ordered mesoporous structure, as it can provide sufficient electrostatic shielding and effective hydrogen bonding, and the solvent evaporation can sometimes assist the self-assembly of molecules. Unfortunately, nonpolar solvents, especially those with high boiling points, have rarely been considered in the synthesis of ordered mesoporous structures because of their negligible interaction with the molecules in the solution and the high temperature necessary to remove them.[4] However, many important functional nanomaterials, for example, PbSe and CdSe, are formed in the oil phase, that is, a nonpolar solvent.[5] Therefore, the extension of the synthesis of mesoporous materials to nonpolar solvents would broaden the scope of materials with ordered mesoporous structures and allow more interesting applications to be explored.

In particular, the combination of porous channels with defined structure and morphology, for example, one-dimensional (1D) nanowires/nanotubes, two-dimensional (2D) nanosheets etc., may induce attractive features for various applications,[6] which, however, have mainly been demonstrated for non-ordered porous structures. Herein, we report a general approach for the synthesis of ultrathin 2D nanoflakes of amorphous transition-metal phosphates, including $FePO_4$, $Mn_3(PO_4)_2$, and $Co_3(PO_4)_2$, with ordered pore channels. The ordered pore channels are aligned with their long axis parallel to the primary surfaces of the nanoflakes. Tetradecylphosphonic acid (TDPA) served as both the structure-directing agent and reactant to generate phosphates of the corresponding organic metal complex (i.e. metal oleate). A vacuum annealing process allows ordered pore channels with an average inner diameter of about 2.5 nm to be prepared in the ultrathin flakes. As a proof-of-concept application of the amorphous metal phosphates, the electrochemical properties of mesoporous $FePO_4$ as a cathode for

[*] D. Yang, Dr. Z. Y. Lu, Dr. X. H. Rui, X. Huang, Dr. H. Li, W. Y. Zhang, Prof. Y. M. Lam, Prof. H. H. Hng, Prof. H. Zhang, Prof. Q. Y. Yan
School of Materials Science and Engineering
Nanyang Technological University
50 Nanyang Aveue, Singapore 637819 (Singapore)
E-mail: hzhang@ntu.edu.sg
alexyan@ntu.edu.sg
D. Yang, Dr. J. X. Zhu, Prof. Q. Y. Yan
TUM CREATE, 1 CREATE Way, no. 10-02 CREATE Tower
Singapore 138602 (Singapore)
Prof. Q. Y. Yan
Energy Research Institute@NTU, Nanyang Technological University
Singapore 637459 (Singapore)

[**] This work was supported by MOE under AcRF Tier 2 (ARC 26/13, no. MOE2013-T2-1-034), AcRF Tier 1 (RG2/13, RG 61/12, RGT18/13, RG5/13), A*STAR SERC grant 1021700144, MPA 23/04.15.03 grant, a Start-Up Grant (M4080865.070.706022) in Singapore, and Singapore National Research Foundation under the CREATE program: EMobility in Megacities. This research is also conducted by NTU-HUJ-BGU Nanomaterials for Energy and Water Management Programme under the Campus for Research Excellence and Technological Enterprise (CREATE) that is supported by the National Research Foundation, Prime Minister's Office, Singapore.

Supporting information for this article (including complete details of the synthesis of metal phosphates with ordered mesoporous structures and characterization methods) is available on the WWW under http://dx.doi.org/10.1002/anie.201404615.

lithium-ion batteries (LIBs) was studied, which delivered a large discharge capacity of 160 mAh g^{-1} for the first cycle and good charge/discharge cycling stability.

As a typical experiment, iron oleate ($Fe(OA)_3$) was prepared by reaction of $FeCl_3$ with sodium oleate (NaOA). Then, 1 mmol $Fe(OA)_3$ and 1 mmol TDPA powder were added to 5 mL 1-octadecene (ODE) solution and the reaction was kept at 300 °C for 1 h. The precipitate was washed several times with hexane, and dried at room temperature. The resulting product was then further annealed in a gas mixture of H_2/Ar at 400 °C for 5 h under vacuum (ca. 10^{-2} torr) to remove excessive surfactant.

To investigate the composition of the obtained product, X-ray photoelectron spectroscopy (XPS) was carried out (see Figure S1 in the Supporting Information). The peaks corresponding to the binding energy of Fe_{2p} appear at 712.6 and 725.7 eV (see Figure S1a in the Supporting Information), which indicates an Fe^{III} state.[7] The P_{2p} (see Figure S1b in the Supporting Information) and O_{1s} spectra (see Figure S2 in the Supporting Information) show the feature peaks at 531.5 and 133.3 eV, respectively, which match the characteristic peaks of $(PO_4)^{3-}$ very well.[7] The Fe/P atomic ratio was 1.05:1 as measured by inductively coupled plasma (ICP) analysis. These results indicate that the as-obtained sample is $FePO_4$. Furthermore, the XPS spectrum for C_{1s} (see Figure S2b in the Supporting Information) and Raman spectra (see Figure S3 in the Supporting Information) confirmed the presence of carbon in the composites. The carbon content was determined to be approximately 30% on the basis of a previously reported method that involved dissolving the sample in a hydrochloric acid solution and weighing the remains.[8]

As shown in the transmission electron microscope (TEM) image (Figure 1a), the obtained $FePO_4$ was composed of interconnected flakes. The ordered continuous channels with uniform diameters in each flake are clearly observed (Figure 1a,b). Atomic force microscopy (AFM) analysis demonstrates the size of the flakes to be in the range of several tens to hundreds of nanometers, and the thickness of a single flake to be about 3.7 nm (Figure 1c,d). The low-angle X-ray diffraction (XRD) pattern for the sample shows four resolved diffraction peaks (Figure 1e). The d values for the four peaks were calculated from Bragg's law ($2d\sin\theta = n\lambda$) to be approximately 3.77, 1.85, 1.28, and 0.96 nm. The ratio of these d values is close to $1:{}^1/_2:{}^1/_3:{}^1/_4$. Therefore, the four peaks can be accordingly indexed as (100), (200), (300), and (400) reflections, thus indicating the highly ordered structure along the [100] direction. As shown in the inset of Figure 1e, the magnified TEM image reveals that the distance between the centers of two neighboring channels (defined as D_{center}) is 3.72 nm, which is highly consistent with the d value (3.77 nm) calculated from the low-angle XRD pattern. Importantly, both the d and D_{center} values are close to the thickness of the flake, as determined by AFM (3.7 nm, Figure 1d), which indicates the $FePO_4$ flakes may consist of only one single layer of pore channels. The wide-angle XRD pattern shows no apparent diffraction peaks (see Figure S4 in the Supporting Information), thus indicating the amorphous nature of the products.

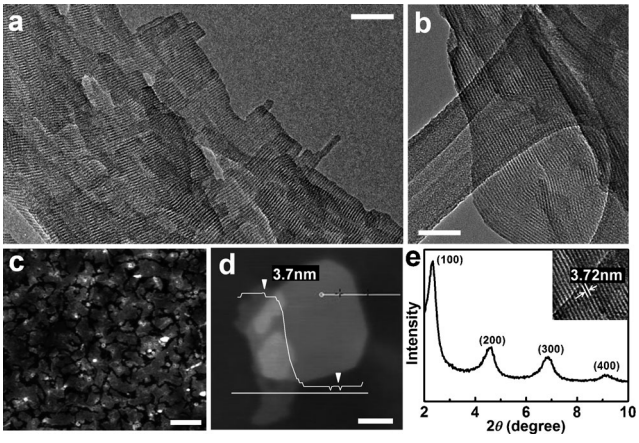

Figure 1. a) Low-magnification TEM image showing the 2D morphology of $FePO_4$ flakes (scale bar: 50 nm). b) Magnified TEM image of a typical $FePO_4$ nanoflake (scale bar: 20 nm). c) Low-magnification AFM image of $FePO_4$ flakes (scale bar: 1 μm). d) AFM image and corresponding height profile of a typical $FePO_4$ nanoflake (scale bar: 20 nm). e) Low-angle XRD pattern of $FePO_4$ flakes (inset: magnified TEM image of $FePO_4$ nanoflake, showing the distance between the neighboring channels is 3.72 nm).

The $FePO_4$ flakes yield type-IV nitrogen adsorption and desorption isotherms with a hysteresis in the middle relative pressures (see Figure S5 in the Supporting Information), which is characteristic of uniform mesopores.[9] The BET surface area is 108 $cm^2 g^{-1}$ and the pore size distribution was calculated by the Barrett–Joyner–Halenda (BJH) model, which showed a narrow peak with a mean value of 2.5 nm (see inset in Figure S5 in the Supporting Information). This value corresponds to the diameter of the channel-shaped pores (defined as d_{pore}). From the values of d_{pore} and D_{center}, the wall thickness of the mesopores, that is, $(D_{center}-d_{pore})/2$, was about 0.6 nm.

Our method is very general. Besides $FePO_4$, this synthetic procedure can be extended to the preparation of manganese and cobalt phosphates, by using $Mn(OA)_2$ and $Co(OA)_2$ as precursors, respectively. XPS results showed the metals are in the Mn^{II} and Co^{II} states, with the representative peak located at 641.2 and 780.2 eV, respectively (see Figures S6 and S7 in the Supporting Information). The presence of PO_4^{3-} was confirmed by the binding energy of P_{2p} being found at around 133 eV (see Figures S6b and S7b in the Supporting Information). ICP measurements showed the Mn/P and Co/P ratio to be 1.47:1 and 1.52:1, which corresponds to the stoichiometric ratios of $Mn_3(PO_4)_2$ and $Co_3(PO_4)_2$, respectively. The low-magnification TEM images (see Figures S8 and S9 in the Supporting Information) showed both samples to have an ultrathin-flake morphology. The shape of the flakes is irregular and their sizes are also not very uniform, ranging from tens to hundreds of nanometers. AFM images (see Figures S10 and S11 in the Supporting Information) showed that the thickness of the $Mn_3(PO_4)_2$ and $Co_3(PO_4)_2$ nanoflakes is 4.0 and 5.2 nm, respectively. The high-magnification TEM images (Figure 2a,b) revealed pore channels in both samples, with their long axes aligned parallel to the primary surfaces of the thin flakes. The D_{center} values were 3.53 and 3.44 nm for $Mn_3(PO_4)_2$ and $Co_3(PO_4)_2$, respectively. The low-angle XRD patterns (Figure 2c,d) showed a series of peaks at 2.46, 4.83,

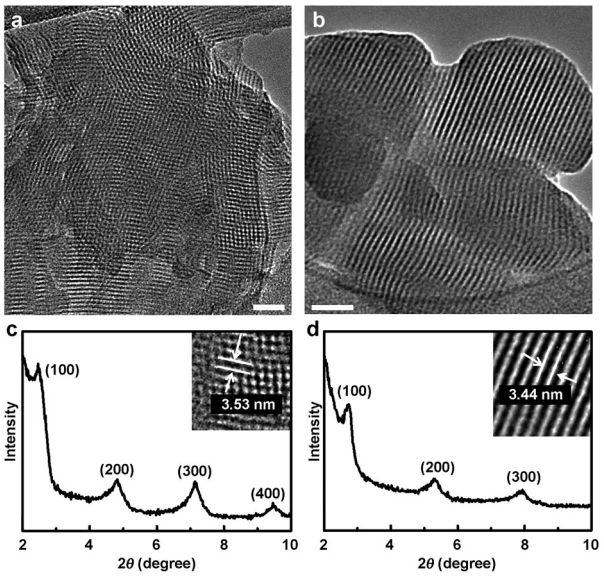

Figure 2. a,b) TEM images (scale bar: 25 nm for (a) and 20 nm for (b)) and c,d) low-angle XRD patterns for the $Mn_3(PO_4)_2$ (a,c) and $Co_3(PO_4)_2$ (b,d) mesoporous structures. Insets in (c) and (d): magnified images of $Mn_3(PO_4)_2$ and $Co_3(PO_4)_2$ samples.

7.13, and 9.48° for $Mn_3(PO_4)_2$, and peaks at 2.72, 5.32, and 7.91° for $Co_3(PO_4)_2$, which correspond to the *d* spacings of 3.58, 1.82, 1.24, and 0.93 nm for $Mn_3(PO_4)_2$ and 3.24, 1.66, and 1.12 nm for $Co_3(PO_4)_2$. The peaks are indexed as (100), (200), (300) ,and (400) for $Mn_3(PO_4)_2$, and (100), (200), and (300) for $Co_3(PO_4)_2$. Low-angle XRD only showed a (100) reflection and its multiples, which indicates that these products contain highly oriented 2D mesostructures, and are in good agreement with the TEM (Figure 2 a,b) and AFM observations (see Figures S10 and S11 in the Supporting Information). Wide-angle XRD showed that $Mn_3(PO_4)_2$ and $Co_3(PO_4)_2$ samples are also amorphous (see Figures S12 and S13 in the Supporting Information). The BET surface areas were determined on the basis of the nitrogen adsorption and desorption isotherms (see Figures S14 and S15 in the Supporting Information) to be 112.8 $m^2 g^{-1}$ for $Mn_3(PO_4)_2$ with a channel diameter of 2.43 nm, and 104.8 $m^2 g^{-1}$ for $Co_3(PO_4)_2$ with a channel diameter of 2.23 nm.

Amorphous $FePO_4$ with a controllable shape and size has attracted great interest as an alternative cathode material for lithium-ion batteries (LIBs), and such a lithium-free cathode is expected to spur the development of LIBs with Li-containing anodes.[10] As a proof of concept, we investigated the cathode performance of amorphous $FePO_4$ with an ordered mesoporous structure for LIBs. Galvanostatic discharge/charge profiles (see Figure S16 in the Supporting Information) revealed a flat plateau around 3.2 V, in accordance with the previous reports.[10a] The first cycle/discharge capacity is 160 mAh g^{-1} and the corresponding charge capacity is 153 mAh g^{-1}, which corresponds to a coulombic efficiency of 95.6 % (1 C is equal to 170 mA g^{-1}). The cycling stability of the sample was studied by charging/discharging the $FePO_4$ electrode at 0.1 C over 100 cycles (Figure 3 a). The discharge capacities stabilized at 140 mAh g^{-1} during the 100th cycle, which corresponds to 82.3 % of the theoretical

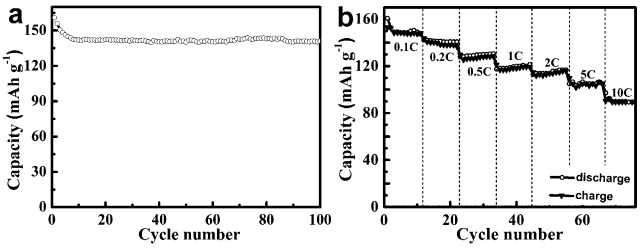

Figure 3. a) Cycling performance of mesoporous $FePO_4$ nanoflakes at 0.1 C. b) Cycling performance of mesoporous $FePO_4$ nanoflakes at different C rates.

value.[10c] The rate capability of the ordered porous thin flakes of $FePO_4$ was also tested (Figure 3 b). The discharge capacity was 149.1, 140.7, 130.6, 120.0, 116.5, 104.9, and 89.4 mAh g^{-1} when the battery was cycled at 0.1, 0.2, 0.5, 1, 2, 5, and 10 C, respectively. Such a good retention of capacity even at a high C rate indicates the excellent rate capabilities of the amorphous $FePO_4$. This excellent cyclic performance may be related to structural features including the ultrathin thickness of the amorphous $FePO_4$ and the ordered mesoporous structure with long channels along its primary surface. Importantly, the TEM image (see Figure S17 in the Supporting Information) showed that the well-defined mesoporous structures of the electrode material were preserved after the cycling test, thus indicating the excellent structure stability of the as-prepared $FePO_4$ flakes. The formation of the ordered mesoporous structure is proposed to originate from the cooperative assembly of composite micelles formed by TDPA and $Fe(OA)_3$, as a result of their amphiphilic molecular structure.[11] When the temperature is high enough to break the Fe–O bond, $Fe(OA)_3$ can react with TDPA to generate $FePO_4$ (see Scheme S1 in the Supporting Information).

To study the formation of the mesoporous structure, the solution was heated to 200 °C, which is lower than the reaction temperature but high enough to ensure the precursors are completely dissolved (the DSC results are shown in Figure S18 in the Supporting Information). The as-heated solution was then cooled to room temperature, but no precipitate could be observed. The structure of the micelles in the solution was studied by small-angle X-ray scattering (SAXS; Figure 4 a), with four resolved peaks being detected. The *q* values were located at 1.68, 3.47, 5.14, and 6.43 nm^{-1}. The *d* values are calculated from the equation $q = 2\pi/d$ to be 3.74, 1.81, 1.22, and 0.98 nm, respectively, which are very close to the *d* values of the amorphous $FePO_4$ flakes measured by low-angle XRD (Figure 1 d). There are two possible structures to explain the SAXS results: 1) the micelles in the solution form lamellar structures with regular periodical spacing,[12] and 2) there is a 2D assembly of cylinder-shaped micelles with mainly the (100) facets exposed. On the basis of the TEM observations discussed above, the second structure is more convincing. The mesoporous $FePO_4$ flakes are likely evolved from the 2D assembly of the cylinderical micelles composed of $Fe(OA)_3$ and TDPA in ODE. Within each cylindrical micelle, the electric dipole could be formed due to the presence of the positively charged Fe^{3+} ion and the deviation of the pore shape from that of a perfect cylinder (Figure 4 c–e).[13] As ODE is a nonpolar solvent, there should

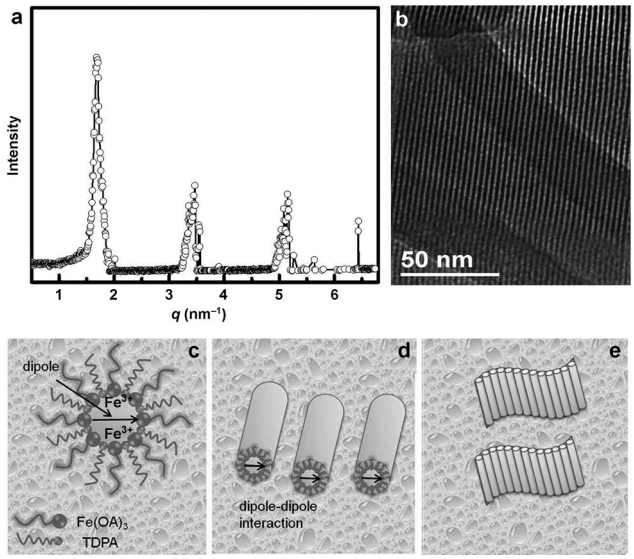

Figure 4. a) SAXS pattern measured for a solution of $Fe(OA)_3$ and TDPA dissolved in ODE without any precipitation. The test was done at room temperature. b) TEM image of the as-prepared sample with an ordered mesoporous structure. c–e) Schematic illustration of the formation of the 2D assembled cylindrical micelles. c) Dipole formation inside each micelle consisting of amphiphilic $Fe(OA)_3$ and TDPA molecules in ODE. d) Linear arrangement of the cylindrical micelles with their long axes aligned parallel to each other through dipole–dipole interactions. e) 2D assembly of cylindrical micelles.

be no ions such as H^+ or OH^- (as in the polar solvent) to interact with the charged groups in the micelles and thus affect the micelle–micelle interaction. Hence, the interaction between each micelle would be more likely related to dipole interactions between micelles. Here, the dipoles present in individual micelles (Figure 4c–e) interact with each other and guide the linear assembly of the cylindrical micelles (Figure 4d) to minimize the enthalpy of the system by promoting dipole alignment and reducing the distance between dipoles. This phenomenon can be regarded as similar to the linear assembly of nanoparticles as a result of dipole–dipole interactions.[14] Here, it is also worth noting that, despite their ordered mesoporous structure (Figure 4b), the metal phosphate nanoflakes are amorphous in nature, thus their 2D construction should not be related to their inherent crystallographic properties like those of layer-structured MoS_2 or graphene sheets.[15] With the aforementioned demonstration that ultrathin 2D nanostructures of transition-metal phosphates could be prepared through a solvothermal reaction process in a nonpolar organic solution, it is expected that the scope of mesoporous materials could be further expanded by similar systems, which may bring about more surprising applications in energy conversion and storage.

Received: April 23, 2014
Published online: July 2, 2014

Keywords: lithium-ion batteries · mesoporous materials · nonpolar solvents · transition-metal phosphates · ultrathin flakes

[1] a) X. He, D. Antonelli, *Angew. Chem.* **2002**, *114*, 222–238; *Angew. Chem. Int. Ed.* **2002**, *41*, 214–229; b) M. E. Davis, *Nature* **2002**, *417*, 813–821; c) P. T. Tanev, M. Chibwe, T. J. Pinnavaia, *Nature* **1994**, *368*, 321–323; d) I. I. Slowing, B. G. Trewyn, S. Giri, V. S. Y. Lin, *Adv. Funct. Mater.* **2007**, *17*, 1225–1236.

[2] a) K. B. Lee, S. M. Lee, J. Cheon, *Adv. Mater.* **2001**, *13*, 517–520; b) S. Jun, S. H. Joo, R. Ryoo, M. Kruk, M. Jaroniec, Z. Liu, T. Ohsuna, O. Terasaki, *J. Am. Chem. Soc.* **2000**, *122*, 10712–10713; c) H. J. Shin, R. Ryoo, Z. Liu, O. Terasaki, *J. Am. Chem. Soc.* **2001**, *123*, 1246–1247; d) F. Jiao, J. C. Jumas, M. Womes, A. V. Chadwick, A. Harrison, P. G. Bruce, *J. Am. Chem. Soc.* **2006**, *128*, 12905–12909.

[3] a) S. Che, A. E. Garcia-Bennett, T. Yokoi, K. Sakamoto, H. Kunieda, O. Terasaki, T. Tatsumi, *Nat. Mater.* **2003**, *2*, 801–805; b) Q. Huo, D. I. Margolese, U. Ciesla, P. Feng, T. E. Gier, P. Sieger, R. Leon, P. M. Petroff, F. Schuth, G. D. Stucky, *Nature* **1994**, *368*, 317–321; c) F. Jiao, A. H. Hill, A. Harrison, A. Berko, A. V. Chadwick, P. G. Bruce, *J. Am. Chem. Soc.* **2008**, *130*, 5262–5266; d) P. Yang, T. Deng, D. Zhao, P. Feng, D. Pine, B. F. Chmelka, G. M. Whitesides, G. D. Stucky, *Science* **1998**, *282*, 2244–2246; e) P. Yang, D. Zhao, D. I. Margolese, B. F. Chmelka, G. D. Stucky, *Nature* **1998**, *396*, 152–155; f) M. J. MacLachlan, N. Coombs, G. A. Ozin, *Nature* **1999**, *397*, 681–684; g) G. S. Armatas, M. G. Kanatzidis, *Science* **2006**, *313*, 817–820.

[4] a) M. A. J. Gillissen, M. M. E. Koenigs, J. J. H. Spiering, J. A. J. M. Vekemans, A. R. A. Palmans, I. K. Voets, E. W. Meijer, *J. Am. Chem. Soc.* **2014**, *136*, 336–343; b) X. Yang, X. Xu, H. F. Ji, *J. Phys. Chem. B* **2008**, *112*, 7196–7202.

[5] a) K. S. Cho, D. V. Talapin, W. Gaschler, C. B. Murray, *J. Am. Chem. Soc.* **2005**, *127*, 7140–7147; b) X. Peng, L. Manna, W. Yang, J. Wickham, E. Scher, A. Kadavanich, A. P. Alivisatos, *Nature* **2000**, *404*, 59–61.

[6] a) A. I. Hochbaum, D. Gargas, Y. J. Hwang, P. Yang, *Nano Lett.* **2009**, *9*, 3550–3554; b) N. Du, H. Zhang, B. D. Chen, J. B. Wu, X. Y. Ma, Z. H. Liu, Y. Q. Zhang, D. R. Yang, X. H. Huang, J. P. Tu, *Adv. Mater.* **2007**, *19*, 4505–4509; c) J. Zhu, Z. Yin, H. Li, H. Tan, C. L. Chow, H. Zhang, H. H. Hng, J. Ma, Q. Yan, *Small* **2011**, *7*, 3458–3464; d) Y. Sun, X. Hu, W. Luo, Y. Huang, *J. Mater. Chem.* **2012**, *22*, 19190–19195; e) C. Zhai, N. Du, H. Zhang, D. Yang, *Chem. Commun.* **2011**, *47*, 1270–1272.

[7] Y. Yin, P. Wu, H. Zhang, C. Cai, *Electrochem. Commun.* **2012**, *18*, 1–3.

[8] X. H. Rui, Y. Jin, X. Y. Feng, L. C. Zhang, C. H. Chen, *J. Power Sources* **2011**, *196*, 2109–2114.

[9] K. S. W. Sing, D. H. Everett, R. A. W. Haul, L. Moscou, R. A. Pierotti, J. Rouquerol, T. Siemieniewska, *Pure Appl. Chem.* **1985**, *57*, 603–619.

[10] a) Y. J. Lee, H. Yi, W. J. Kim, K. Kang, D. S. Yun, M. S. Strano, G. Ceder, A. M. Belcher, *Science* **2009**, *324*, 1051–1055; b) Y. S. Hong, K. S. Ryu, Y. J. Park, M. G. Kim, J. M. Lee, S. H. Chang, *J. Mater. Chem.* **2002**, *12*, 1870–1874; c) Y. Yin, Y. Hu, P. Wu, H. Zhang, C. Cai, *Chem. Commun.* **2012**, *48*, 2137–2139; d) S. W. Kim, J. Ryu, C. B. Park, K. Kang, *Chem. Commun.* **2010**, *46*, 7409–7411.

[11] F. Zhang, Y. Meng, D. Gu, Y. Yan, Z. Chen, B. Tu, D. Zhao, *Chem. Mater.* **2006**, *18*, 5279–5288.

[12] D. Myers, *Surfactant Science and Technology*, Wiley-Interscience, Hoboken, NJ, **2006**.

[13] J. Nappa, G. Revillod, I. Russier-Antoine, E. Benichou, C. Jonin, P. F. Brevet, *Phys. Rev. B* **2005**, *71*, 165407.

[14] a) Z. Tang, N. A. Kotov, M. Giersig, *Science* **2002**, *297*, 237–240; b) M. Shim, P. Guyot-Sionnest, *J. Chem. Phys.* **1999**, *111*, 6955–6964.

[15] a) S. Wu, Z. Zeng, Q. He, Z. Wang, S. J. Wang, Y. Du, Z. Yin, X. Sun, W. Chen, H. Zhang, *Small* **2012**, *8*, 2264–2270; b) H. Wang, J. T. Robinson, X. Li, H. Dai, *J. Am. Chem. Soc.* **2009**, *131*, 9910–9911.

